Published by IOP Publishing for Sissa Medialab

Received: *February 2, 2020*
Accepted: *February 18, 2020*
Published: *April 8, 2020*

15TH Topical Seminar on Innovative Particle and Radiation Detectors
14–17 October 2019
Siena, Italy

The BDX detector prototype for dark matter searches in a Beam Dump eXperiment at JLAB

M. Bondí,[a,1] **M. Battaglieri,**[b,f] **A. Celentano,**[b] **M. De Napoli,**[a] **R. De Vita,**[b] **L. Marsicano,**[b,e] **A. Italiano,**[a] **N. Randazzo,**[a] **V. Sipala**[c,d] **and E. Smith**[f]

[a] *INFN, Sezione di Catania, Via S. Sofia 64, I-95125 Catania, Italy*
[b] *INFN, Sezione di Genova, Via Dodecaneso 33, I-16146 Genova, Italy*
[c] *Università degli Studi di Sassari, Via Vienna 2, I-07100 Sassari, Italy*
[d] *INFN, Laboratori Nazionali del Sud, Via S. Sofia 62, I-95125 Catania, Italy*
[e] *Dipartimento di Fisica, Università degli Studi di Genova, Via Dodecaneso 33, I-16146 Genova, Italy*
[f] *Jefferson Lab, Newport News, VA 23606, U.S.A.*

E-mail: mariangela.bondi@ct.infn.it

Abstract: The Beam Dump eXperiment (BDX) is an electron-beam thick-target experiment aimed to investigate the existence of light dark matter particles in the MeV-GeV mass range at Jefferson Lab. A small-scale prototype (BDX-Proto) of the BDX detector has been constructed in order to validate the proposed design and to demonstrate with real measurements the capability to efficiently reject the cosmogenic backgrounds. In this paper we report the peformance of BDX-Proto extracted from a long campaign of cosmic ray measurements performed at INFN, Sez. Catania and INFN, LNS.

Keywords: Calorimeters; Photon detectors for UV, visible and IR photons (solid-state) (PIN diodes, APDs, Si-PMTs, G-APDs, CCDs, EBCCDs, EMCCDs, CMOS imagers, etc); Scintillators, scintillation and light emission processes (solid, gas and liquid scintillators)

[1] Corresponding author.

https://doi.org/10.1088/1748-0221/15/04/C04022

Contents

2020 JINST 15 C04022

1 Introduction

Nowadays deciphering the fundamental nature of dark matter (DM) is one of the foremost open questions in fundamental science. The dark matter experimental program is mainly focused on weakly-interacting massive particles (WIMPs), but in the recent years many innovative dark matter candidates have emerged. One of them conjectures the existence of DM particles in MeV-GeV mass range. They are charged under a new $U(1)_D$ broken symmetry, whose vector boson mediator A' (heavy or dark photon) is massive. The dark photon can be kinetically mixed with the standard model (SM) hypercharge field, resulting in SM-DM interaction [1]. This scenario stimulated many theoretical studies, triggering new experimental programs to search both for the A' and for light DM states [2]. Among them, an accelerator-based experiment where an intense electron beam of moderate energy (~10 GeV) is dumped on a beam-dump can greatly improve the sensitivity to sub-GeV DM [3].

BDX (Beam Dump eXperiment) is an experiment aimed to search for light DM particles produced in a beam-dump at Jefferson Lab [4]. It is expected to run in a dedicated underground facility located ~ 20 m downstream of the JLab-Hall A beam-dump. Hall-A can receive from the JLab-CEBAF accelerator an 11 GeV electron beam with a maximum current of ~ 65 μA. Such high intensity allows to reach the BDX goal of collecting 10^{22} electron-on-target (EOT) in ~ 285 days of full parasitic run. Dark photons can be produced by the interactions of the e^--beam in the dump via A'-strahlung processes [1] and e^+e^- annihilations [5]. They can then decay into forward-boosted DM particles (χ) that can reach the BDX detector crossing the concrete and iron shielding placed after the dump to suppress the beam-related SM background (except neutrinos). In particular, BDX is looking for $\chi - e^-$ scattering resulting in a high-energy scattered e^-. In order to be sensitive to

this interaction channel, the BDX detector consists of two main components: an electromagnetic calorimeter (ECAL) and a Veto system used to reject the background. Therefore the expected DM signature is an high-energy (~ GeV) EM shower paired with a null activity in the surrounding vetos. A sketch of the experimental set-up is shown in figure 1.

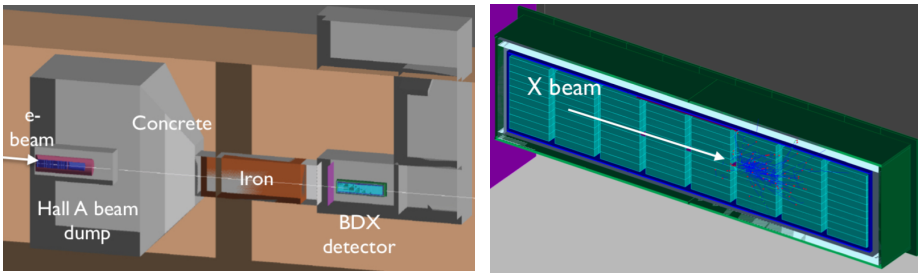

Figure 1. Left panel: the BDX experimental setup. Right panel: a GEANT4 implementation of the BDX detector.

The ECAL consists of 8 modules of 10×10 CsI(Tl) crystals each, arranged with the long size along the beam direction. The average size of each crystal is $4.7 \times 5.4 \times 32.5\,\mathrm{cm}^3$. This arrangement has a cross section of $\sim 50 \times 55\,\mathrm{cm}^2$ and a total length of ~ 3 m with excellent forward geometric acceptance. Silicon Photo-multipliers (SiPMs) are used as light-readout sensors. The detector will be placed at the beam-dump level, i.e. 8 m underground with ~10 meters of water equivalent (mwe) overburden. The ECAL is operated inside two hermetic layers of active veto counters made of large-area plastic-scintillator paddles: the outermost called Outer Veto (OV) and the innermost Inner Veto (IV). In both veto systems light is read-out by SiPMs after being collected through WaveLength Shifting (WLS) fibers (in the IV) and WLS plastics (in the OV). A lead vault, 5 cm thick, is placed between the ECAL and the Vetos to reduce the number of e.m. showers produced by $\chi - e^-$ interaction that may hit the vetoes lowering the signal efficiency.

2 The BDX prototype detector

The BDX detector concept, described in the previous section, has been validated using a small scale ($\sim 1 \times 1.1 \times 1.8\,\mathrm{m}^3$) prototype (BDX-Proto) in a campaign of cosmic-ray measurements at INFN, Sezione di Catania (INFN-CT) and Laboratori Nazionali del Sud (LNS). Figure 2 shows the prototype assembled at INFN-CT (panel C). The different components of BDX-Proto are described in details in the following subsections.

2.1 Electromagnetic calorimeter

The ECAL prototype is made by 16 CsI(Tl) crystals assembled in a 4×4 matrix, as shown in figure 2-panel A. Each crystal, originally employed in the BaBar ECAL [6], is wrapped in a white, diffusive reflector material (Tyvek), then in aluminum and Mylar for light-proofing and insulation, and is inserted inside a regular-parallelepiped aluminum holder ($5 \times 5.5 \times 33\,\mathrm{cm}^3$) providing mechanical protection and the possibility to stack one crystal on top of the other forming the final matrix. Each crystal is read by a $6 \times 6\,\mathrm{mm}^2$ Hamamatsu MPPCs (S13360-6025PE) placed in the middle of the front-face and coupled to it with optical grease. The bias voltage is provided by a custom-designed board [9]. Each sensor is coupled to a trans-impedance amplifier with a gain factor of 50.

2020 JINST 15 C04022

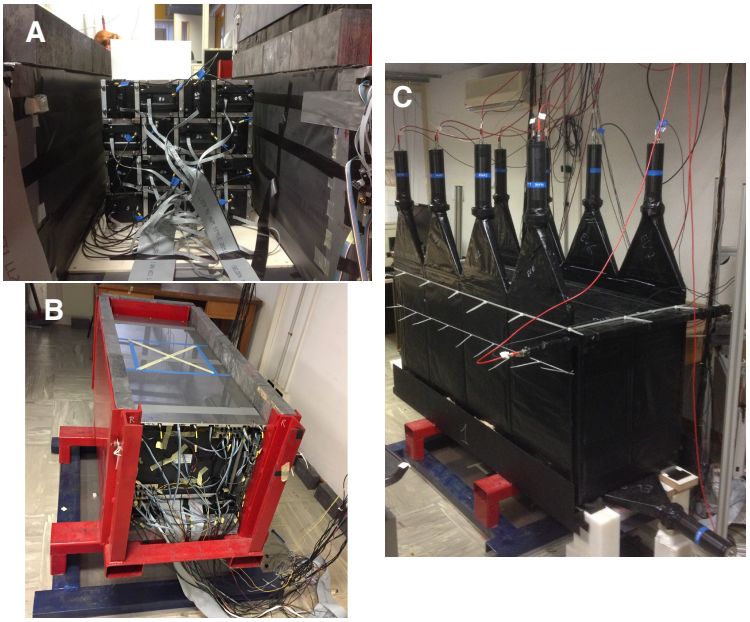

Figure 2. Panel A: ECAL prototype mounted inside BDX-Proto. Panel B: the IV assembled inside the mechanical structure of the prototype. Panel C: the BDX prototype mounted and cabled at INFN-CT.

It is worth mentioning that, although the ECAL prototype was designed to be sensitive to energy deposition of tens of MeV or more, the response of a single CsI(Tl) crystal coupled to a SiPMs to a low energy proton beam has been measured [7]. Results proved that this technology is sensitive to energy depositions as low as 2.5 MeV.

2.2 Inner veto

The IV consists of six EJ200 plastic scintillator paddles, 1 cm thick, forming a nearly hermetic parallelepiped (figure 2-panel B). Grooves on the surface of the scintillators host two WLS fibers each (Φ = 1 mm) to convoy the scintillation light to SiPMs, mounted at the edges. Four $35 \times 140\,\mathrm{cm}^2$ scintillators form the top, bottom, left and right sides of the veto. In each paddle the WLS fibers are inserted into four linear grooves running parallel to the long side of the plastic, each one ending into a SiPM (Hamamatsu S12572-100 C). Thanks to the light transmission inside the clear plastic, any energy deposition in the paddle results in a visible signal at each SiPM, providing high redundancy in the readout. This makes any single SiPM inefficiency negligible, and also allows to use reduced thresholds in the analysis, by exploiting time coincidence between different SiPM signals.

The upstream and downstream caps, instead, are made by a smaller paddle ($35 \times 42\,\mathrm{cm}^2$) with a spiral grove, coupled to a single SiPM. For all IV SiPMs, the bias voltage and the signal amplification are provided by the same custom-designed boards and amplifiers (with gain=160) used for the ECAL.

2.3 Outer veto

Large-area plastic scintillator paddles form the OV (figure 2-panel C). Thanks to the lower geometrical requirements, different readout solutions based on WLS scintillator bars coupled to PMTs,

2020 JINST 15 C04022

and the more space-demanding light-guides coupled to PMTs, were tested. This allowed to make a comparison between the different solutions in preparation to the final design.

The bottom and lateral sides are made by ten $80 \times 40\,\mathrm{cm}^2$ NE110 plastic scintillators, 2 cm thick. A fish-tail shaped PMMA light-guide, glued on one side of each scintillator, directs the light to a 2 inch photomultiplier tube (Thorn EMI 9954A) optically matched to the light-guide with optical grease.

Top, upstream and downstream sides are made by EJ200 scintillators, 2.5 cm thick. The upstream (downstream) and top paddles have an area of $58 \times 66\,\mathrm{cm}^2$ and $184 \times 54\,\mathrm{cm}^2$, respectively. The use of a long single piece of plastic scintillator to cover the top side is meant to avoid dead spaces coming from the junctions between different paddles. In this case light is readout from the two opposite edges of the paddle, so to avoid potential detection inefficiencies related to light attenuation along to the significant length of the scintillator. In the top and upstream (downstream) scintillators light-guides are replaced by EJ280 WLS bars [8] that absorb and remit light within line-of-sight of a PMT. Each scintillator paddle is diamond milled on all sides, except for one (two in case of the top layer) that is instead 'frosted' by sandpaper and where the WLS bar is mechanically matched offset by an air gap of ~ 0.5 mm. This configuration provides a uniform, diffuse spread of scintillation light along the length of the WLS bar followed by the air gap which subsequently aids in preventing wavelength-shifted light from escaping the wave-length shifter by exploiting total internal reflection. At the end of the WLS strip is a 2.5 cm in diameter Hamamatsu R1924A PMT for light collection.

3 Cosmogenic background measurements

In this section we report the results of the cosmogenic background measurements performed with the BDX prototype. Thanks to these measurements we could finalize the design of the full detector, make realistic predictions of its expected performances and, ultimately, establish the expected cosmic background contribution to the sensitivity of the BDX experiment.

3.1 Data acquisition and reconstruction

Each signal from the detector was split into two equal copies by a 1:1 passive splitter. The first was sent to a FADC board, and the second to a leading-edge discriminator. The digital signals from the discriminator boards (CAEN V895) were sent to a FPGA board (CAEN V1495), implementing the trigger logic. The main trigger condition required a single signal from any CsI(Tl) crystal to pass a 5 photo-electrons (phe) threshold. The whole readout system was handled through the "Cebaf Online Data Acquisition" (CODA).

The reconstruction code to handle the BDX-Proto data was developed in the "JLab Data Analysis Framework" (JANA). The following data reconstruction procedure was adopted. For each CsI(Tl) crystal, the signal waveform was numerically integrated within a 1 µs time window to obtain the corresponding charge. This was converted in MeV units by using calibration constants deduced from the most probable value of the cosmic-rays Landau distribution. In particular, in order to calibrate in energy each crystal, only the most vertical tracks, selected requiring a four-fold coincidence between four crystals in the same column, were used. For the IV scintillators with multiple readout (top, bottom, left and right) we required, after numerical integration of the

2020 JINST 15 C04022

waveforms within 1 µs time window, that at least two SiPMs of the same paddle collect more than 2.5 phe each, within a coincidence gate of 100 ns. The corresponding rate of false-positive signals due to SiPM thermal rate, evaluated through a dedicated random-trigger run, was found to be $\simeq$ 5% of the total. For the IV counter with a single SiPM a higher threshold ($\sim$ 12.5 phe) was implemented to keep the contribution of false positive signals at similar rate as for the other counters. For the OV detectors signals were first integrated in 1 µs, then calibrated in energy and finally selected applying a 100 keV energy threshold. Before being mounted in the BDX-proto, the response uniformity of each OV paddle was assessed by measuring the response to cosmic ray tracks selected through a small telescope, made of two plastic scintillator counters. Different measurements were taken by changing the telescope position relative to the paddles.

An example of energy spectra extracted after data reconstruction for the ECAL and the Vetos are shown in figure 3.

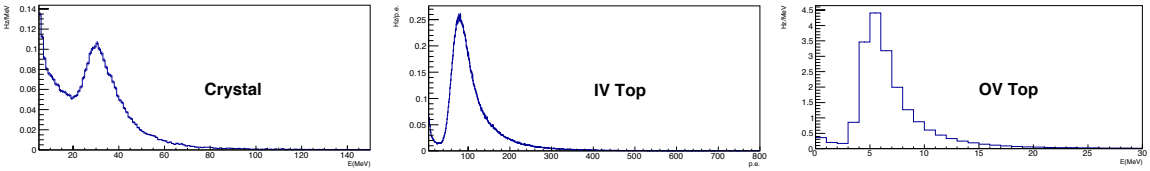

Figure 3. Measured event rate as a function of deposited energy in a CsI(Tl) crystal of the matrix (left panel) and in the top paddle of the IV (in photo-electrons, middle panel) and of the OV (right panel).

3.2 Characterization of cosmic events in the ECAL

In order to benchmark the data and the reconstruction procedure we decided to compare the rate of cosmic muons as a function of the deposited energy in each crystal of the ECAL with the values predicted by Monte Carlo simulations. For this comparison we focused on a very clean class of events, i.e. nearly perpendicular muons crossing the ECAL. Such events have been selected by requiring the presence of a 4-fold coincidence between the four crystals of the same ECAL column and a null activity in the rest of the calorimeter. Figure 4 shows the Landau distribution of the measured event rate as a function of the deposited energy for all the crystals of the ECAL. The measured rates agree very well with the expected values extracted using GEANT4 simulations.

The footprint of cosmic ray events hitting the ECAL have been studied using three different measurable quantities: the highest energy measured in a single crystal per event (E_{seed}), the total energy measured in the ECAL per event (E_{TOT}) and the crystal multiplicity defined as the number of crystals fired (i.e. having a signal over threshold) per event (N_{hits}).

Figure 5 shows the correlation between E_{Tot} and E_{seed} both for all the events (left panel) and requiring the anti-coincidence of the two veto systems (right panel), i.e. for events with no activity in any of the veto counters. In both cases, low-energy events are predominantly distributed along the bisector where $E_{Tot} = E_{seed}$. This results indicate that events where a relatively small amount of energy is released in the ECAL are mainly characterized by the presence of just one hit. However, when the anti-coincidence is required, most of the events lies in the $E_{Tot} = E_{seed}$ bisector almost independently from the energy.

2020 JINST 15 C04022

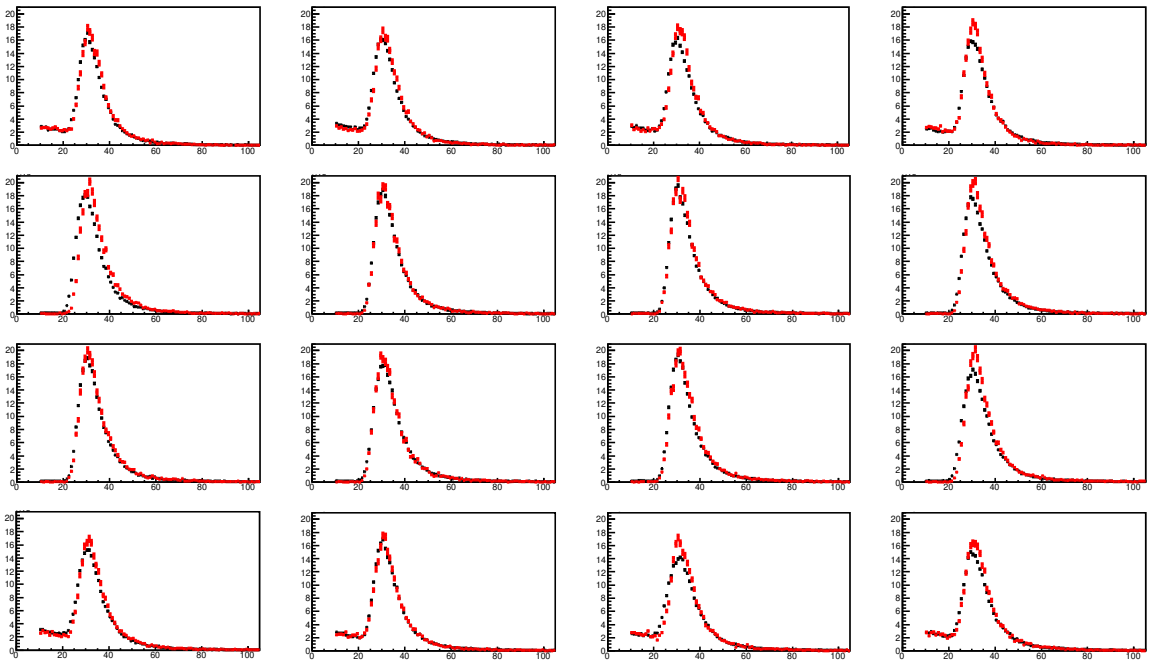

Figure 4. The measured event rate (vertical axis, in mHz/MeV) as a function of deposited energy (horizontal axis, in MeV) in each crystal for selected events where all the crystals of the corresponding column have a signal over a 10-MeV threshold. The black points are the experimental data while the red ones the MC simulations.

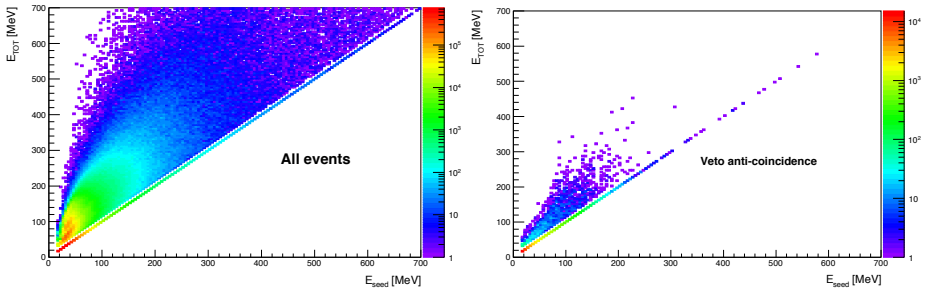

Figure 5. E_{TOT} versus E_{seed} for all events (left panel) and requiring the anti-coincidence of the two veto systems (right panel).

The distribution of the crystal multiplicity as a function of the frequency is shown in figure 6 for different classes of events. Without any condition (class of events a) the distribution is dominated by small multiplicities, with one or two crystals fired in ~ 70 % of the events, and higher multiplicities are exponentially suppressed. This result reflects the fact that most of the data are characterized by low-energy events in the ECAL. Indeed, when high energy events (i.e. E_{seed} >350 MeV are selected (class of events b) the multiplicity distribution shifts toward higher values and peaks at $N_{hits} = 4/5$. A different trend is observed for events that survives Vetoes rejection. With Vetoes in anti-coincidence (class of events c) almost the totality of the events, about 95 %, present only one crystal fired. However, when a high-energy deposition is also required (class of events d) the distribution does not change significantly. Therefore high-energy events (those of interest for BDX)

2020 JINST 15 C04022

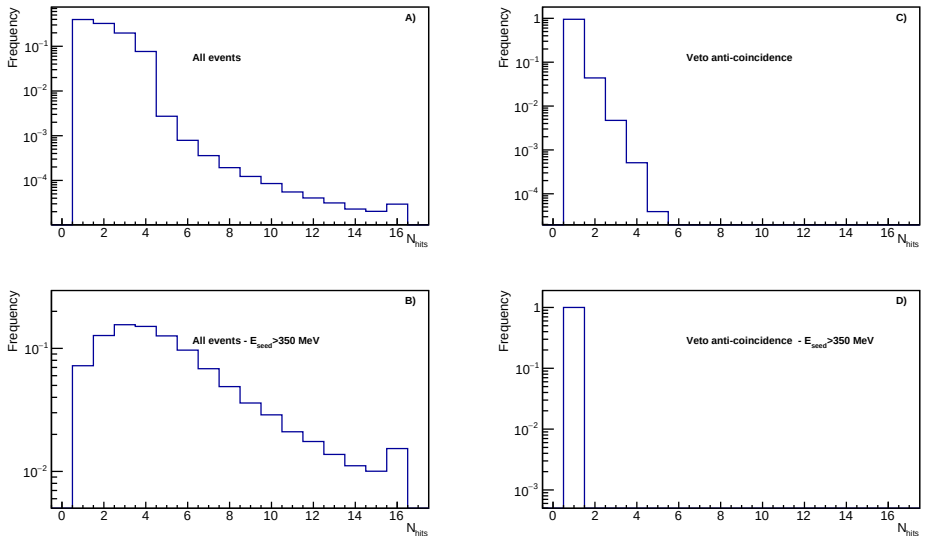

Figure 6. Crystal multiplicity distributions for different classes of events: a) all events, b) high-energy events (i.e. E_{seed} >350 MeV), c) events with no activity in the Vetos, d) high-energy events (i.e. E_{seed} >350 MeV) with no activity in the Vetos.

that escape Veto rejection are characterized by a clear topology: almost all the energy is released inside just one crystal.

3.3 IV and OV performances

The performances of Veto systems have been studied along two directions: on one side by considering events with different and well defined topologies in the ECAL and, on the other side, by focusing on high-energy events. The overall efficiency of each veto system is defined as:

$$\text{Efficiency} = \frac{N_{\text{veto}}}{N_{\text{skimmed}}} \tag{3.1}$$

where N_{skimmed} is the total number of skimmed events, i.e. of the specific class of events considered depending on topology or energy, and N_{veto} is the number of skimmed events presenting a hit on at least one paddle of the Veto system considered (IV or OV). The measured detection efficiency is shown in figure 7, together with a schematic representation of the selected event topologies. The two Vetoes show the same efficiency and, in both cases, the efficiency does not depend on the considered event topology. The high detection efficiency measured >99.5% is a clear evidence of the overall goodness of both systems in terms of hermeticity and proposed solutions.

The background rejection efficiency as a function of event energy is shown in figure 8. The differential rate of events measured in the ECAL versus E_{seed} is reported for the following conditions: all events (black), events with OV (green), IV (red) and both Vetos (blue) in anti-coincidence.

The MIP peak centered at ∼33 MeV is clearly visible in the "All events" spectrum. When the anti-coincidence of one of the two Vetoes is required, then that peak disappears. At the MIP energy the differential counting rate is reduced by a factor ∼ 300 by the OV, a factor ∼ 400 by the IV and a factor ∼ 700 when both vetoes in anti-coincidence are required.

2020 JINST 15 C04022

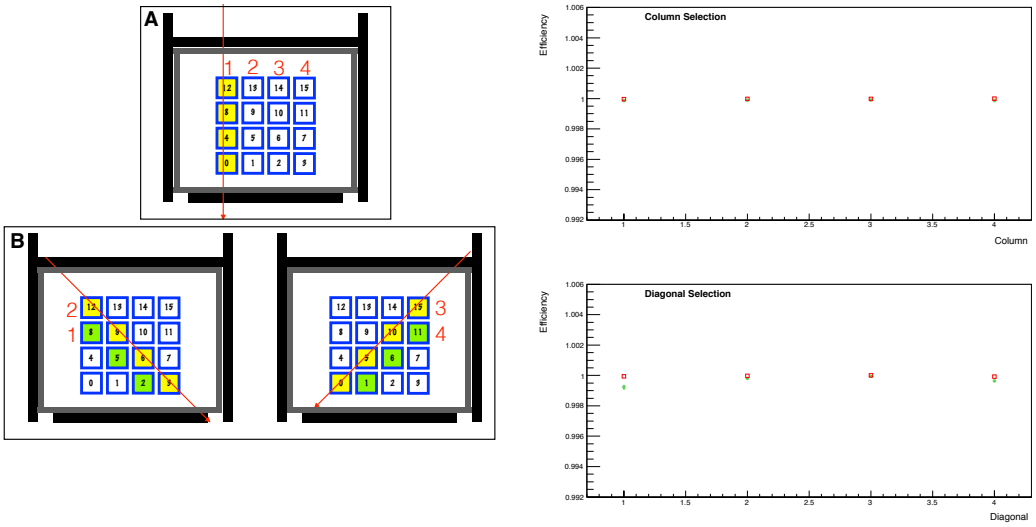

Figure 7. Left panel: A): vertical selection. 1,2,3 and 4 indicates the column number (e.g. column number 1 is made by crystals number 12,8,4,0). B): diagonal selection. As for the columns, different diagonals are named 1,2,3 and 4 following the scheme reported in the figure. Right panel. Top: efficiency as function of the selected column. Bottom: efficiency as function of the selected diagonal. In both cases: green squares refer to OV and red dots to IV.

At higher energies (E_{seed} >350 MeV), i.e. the ones of interest for BDX, the integrated background rate is suppressed by three orders of magnitude. In particular, the total integrated event rate reduces from $2.8 \cdot 10^{-2}$ Hz to $1.1 \cdot 10^{-4}$ Hz, $4.6 \cdot 10^{-5}$ Hz and $2.3 \cdot 10^{-5}$ when using the OV, IV and both vetoes in anti-coincidence, respectively.

3.4 Background rejection results

The total number of cosmogenic background events expected in the BDX experiment has been estimated using BDX-Proto. For this purpose the prototype was placed into a bunker at LNS with a surrounding overburden of about 5 meters of concrete corresponding to an effective thickness of 1080 g/cm^2 which is similar to 1165 g/cm^2 expected at JLab. During these measurements we could instrument only one CsI(Tl) crystal, a non-critical issue since measurements performed with the full ECAL prototype show a dominant multiplicity of one crystal for events selected in anti-coincidence with Vetos. Moreover, the extrapolation to the full BDX experiment has been performed by scaling the single crystal rate to the 800 crystals comprising the full detector. This is certainly an upper limit on the expected rates since this assumes crystal-to-crystal fully uncorrelated counts, which overestimates the case for χ-e$^-$ scattering. The rate of measured high-energy events has been extracted from the best-fit of the high-statistics low-energy region of the spectrum, obtained imposing the IV in anti-coincidence condition (figure 9). In this way we could extract a robust estimation of the number of rare high-energy events without being dominated by statistical uncertainties (figure 9). The systemics associated with this procedure has been evaluated by changing the fit range and comparing the obtained results. The extracted rate for an energy threshold of E_{seed} >350 MeV is $(1.9 \pm 0.9 \cdot 10^{-12})$ Hz that, extrapolated to the full detector, corresponds to $(1.5 \pm 0.7 \cdot 10^{-9})$ Hz. Integrating over the expected beam-on time of the full experiment (285 days) less than (0.037 ± 0.017) projected counts are expected.

2020 JINST 15 C04022

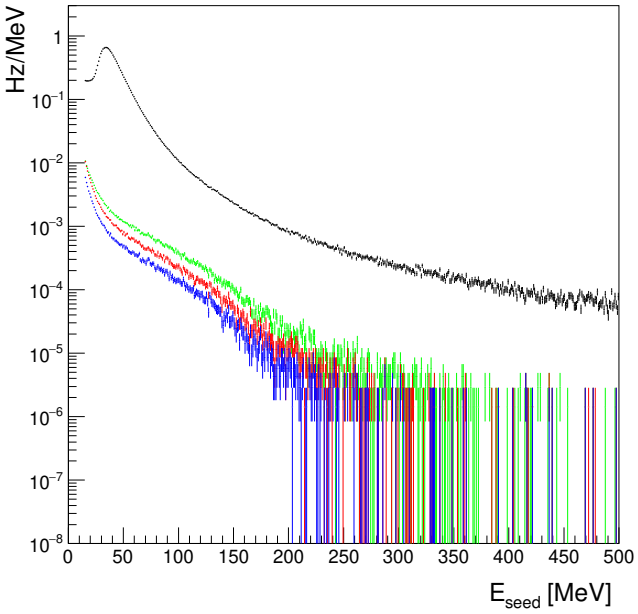

Figure 8. Measured event rate as a function of the energy seed. Different colors refer to the different class of events: black — all events, red — anti-coincidence with IV, green — anti-coincidence with OV, blue — anti-coincidence with both veto systems.

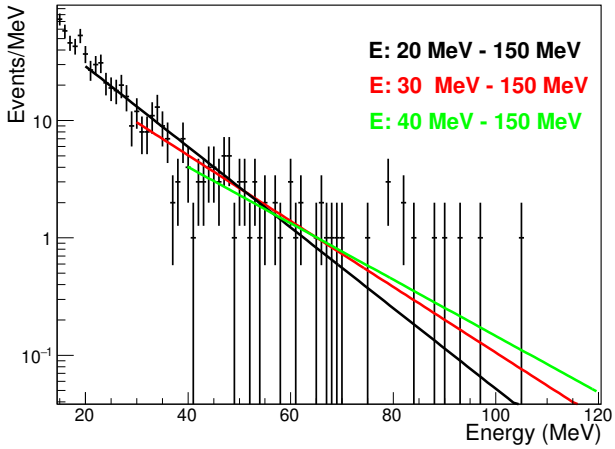

Figure 9. Extrapolation of the measured CsI energy spectrum in anti-coincidence with the inner veto from the low-energy region, where a non-zero event rate was measured, to the high energy region, where no events were detected. The three curves refer to Maximum Likelihood fits performed in different energy ranges.

4 Summary and conclusions

We have designed and constructed the prototype of a detector that can be efficiently used to search for light Dark Matter in an electron beam-dump experiment. The two main characteristics of such detector are: the possibility of detecting e.m. showers produced by $\chi - e^-$ scattering, and the capability to efficiently reject the high-energy cosmogenic background, a particularly critical point for these accelerator-based experiments that can run only with a limited amount of overburden.

2020 JINST 15 C04022

A dedicated campaign of cosmogenic background measurements allowed us to study the performances of the prototype, to validate the technological solutions adopted and to demonstrate the possibility of rejecting the cosmogenic backgrounds. The most significant results of these measurements can be summarized as follow. The quantity E_{seed}, the highest energy measured in a single crystal per event, can be efficiently used in data analysis to remove a large fraction of background events and select only high-energy events, those of interest for BDX. Thanks to their hermeticity and high detection efficiency, the two veto systems are able to reject up to one part in a thousands events with E_{seed} >350 MeV. Events of such energy which survive the veto rejection show a multiplicity in the ECAL that is mostly typically equal to one.

Finally, the background rejection results reported in this paper demonstrate that the proposed setup and analysis strategies are able to reduce to zero the cosmogenic background events that can mimic DM interaction in the BDX experiment.

Acknowledgments

The authors wish to thank the INFN-CT and INFN-GE technical staff for the excellent work done in constructing the detector and Prof. William Wisniewski for providing the CsI(Tl) crystals.

References

[1] B. Holdom, *Two* U(1)*'s and Epsilon Charge Shifts*, *Phys. Lett.* **166B** (1986) 196.

[2] M. Battaglieri et al., *US Cosmic Visions: New Ideas in Dark Matter 2017: Community Report*, in *U.S. Cosmic Visions: New Ideas in Dark Matter*, College Park, MD, U.S.A., 23–25 March 2017 (2017) [arXiv:1707.04591].

[3] E. Izaguirre, G. Krnjaic, P. Schuster and N. Toro, *New Electron Beam-Dump Experiments to Search for MeV to few-GeV Dark Matter*, *Phys. Rev.* **D 88** (2013) 114015 [arXiv:1307.6554].

[4] BDX collaboration, *Dark Matter Search in a Beam-Dump eXperiment (BDX) at Jefferson Lab*, arXiv:1607.01390.

[5] L. Marsicano et al., *Novel Way to Search for Light Dark Matter in Lepton Beam-Dump Experiments*, *Phys. Rev. Lett.* **121** (2018) 041802 [arXiv:1807.05884].

[6] BaBar collaboration, *The BaBar detector*, *Nucl. Instrum. Meth.* **A 479** (2002) 1 [hep-ex/0105044].

[7] M. Bondí et al., *Large-size CsI(Tl) crystal read-out by SiPM for low-energy charged-particles detection*, *Nucl. Instrum. Meth.* **A 867** (2017) 148.

[8] K.J. Thomas, E.B. Norman, A.R. Smith and Y.D. Chan, *Installation of a muon veto for low background gamma spectroscopy at the LBNL low-background facility*, *Nucl. Instrum. Meth.* **A 724** (2013) 47.

[9] A. Celentano, et al., *The High Voltage Regulator Board for the BDX Experiment*, Tech. Rep. INFN-17-03/GE.

2020 JINST 15 C04022